New Joint Demosaicing and Zooming Algorithm for Color Filter Array

Kuo-Liang Chung, *Senior Member*, IEEE, Wei-Jen Yang, Pang-Yen Chen, Wen-Ming Yan, and Chiou-Shann Fuh, *Member*, IEEE

Abstract — *This paper presents a new joint demosaicing and zooming algorithm for digital cameras, each equipped with a single CCD/CMOS sensor and a color filter array (CFA). According to the proposed adaptive heterogeneity projection masks and Sobel- and luminance estimation-based masks, we can extract edge information of each pixel in terms of the direction of variation and the gradient from the mosaic image directly and accurately, and the extracted more accurate edge information will be utilized to assist the design of our proposed new joint demosaicing and zooming algorithm. Based on twenty-four popular testing mosaic images, our proposed new zooming algorithm has better image quality performance in terms of two objective color image quality measures, the color peak signal-to-noise ratio (CPSNR) and the S-CIELAB* ΔE^*_{ab} *metric, and one subjective color image quality measure, the color artifacts, when compared with several previous zooming algorithms.* [1]

Index Terms — Color filter array, Demosaicing algorithm, Digital cameras, Mosaic images, Zooming algorithm.

I. INTRODUCTION

Recently, the digital camera has become more and more popular in the consumer electronics market. In order to reduce the manufacturing cost, instead of using three sensors for each pixel, most manufacturers use a single CCD/CMOS sensor imaging pipeline [19] coated with the well-known Bayer CFA [2] to capture the color information. In Bayer CFA structure, each pixel in the captured image records only one of the three primary colors and this kind of image is called the mosaic image. The depiction of Bayer CFA structure is illustrated in Fig. 1. In Bayer CFA, because the green (G) channel information is the most important factor to determine the luminance of the color image, the number of pixels that records G channel information is twice as that of red (R) channel information and blue (B) channel information. R and B channels which share the rest half of the pixels are considered the chrominance of the image.

[1] This work is supported by the National Science Council of R. O. C. under contract NSC97-2221-E-011-102-MY3.

Kuo-Liang Chung is with the Department of Computer Science and Information Engineering National Taiwan University of Science and Technology No. 43, Section 4, Keelung Road, Taipei, Taiwan 10672, R. O. C. (e-mail: k.l.chung@mail.ntust.edu.tw).

Wei-Jen Yang, Pang-Yen Chen, Wen-Ming Yan, and Chiou-Shann Fuh are with the Department of Computer Science and Information Engineering National Taiwan University No. 1, Section 4, Roosevelt Road, Taipei, Taiwan 10617, R. O. C. (email: {f93035, r95043, ganboon, fuh}@csie.ntu.edu.tw).

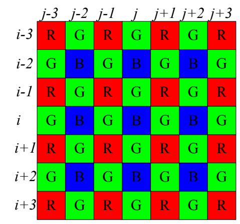

Fig. 1. The Bayer CFA structure.

As indicated above, each pixel of the captured image contains only one of the three primary color information. The process of recovering the two missing color components of the mosaic image is called the demosaicing process [1], [3], [4], [7], [9], [11], [12], [13], [14], [15], [20], [22], [23], [25], [27], [28]. Besides the demosaicing process, the most commonly used operation is the zooming process. In the previously developed zooming algorithms, they all focus on the quad-zooming process. Thus, we follow this kind of zooming process in this research.

Previously, several zooming algorithms on mosaic images have been developed. The previously developed zooming algorithms can be roughly classified into three approaches. In the first approach, the mosaic image is first recovered to the full color image by using the demosaicing process and then the demosaiced full color image is zoomed by using the zooming process [26], [29]. In the first approach, the demosaicing and zooming processes are performed separately and independently. Alternatively, Lukac *et al.* [17], [18] proposed the second approach. In this approach, the mosaic image is first using the CFA zooming method to obtain the zoomed mosaic image, and then the existing demosaicing method is applied to obtain the zoomed full color image. Recently, the third approach using joint demosaicing process and zooming process was proposed by Chung and Chen [5] and Zhang and Zhang [30] simultaneously. Experimental results showed that the third approach has better quality performance when compared with the other two approaches.

In this paper, according to the adaptive heterogeneity projection masks and Sobel- and luminance estimation-based (SL-based) masks [7], we first extract edge information of each pixel in terms of the direction of variation and the gradient from the mosaic image directly and accurately. The extracted edge information can be utilized to assist the design of our proposed new joint demosaicing and zooming algorithm. The detailed flowchart of the proposed joint demosaicing and zooming algorithm is illustrated in Fig. 2. Based on twenty-four popular testing mosaic images, our proposed zooming algorithm has better image quality performance when compared with the previous zooming algorithms which cover the algorithm combining the mosaic

Contributed Paper
Manuscript received June 8, 2009

0098 3063/09/$20.00 © 2009 IEEE

Authorized licensed use limited to: National Taiwan Univ of Science and Technology. Downloaded on October 13, 2009 at 22:45 from IEEE Xplore. Restrictions apply.

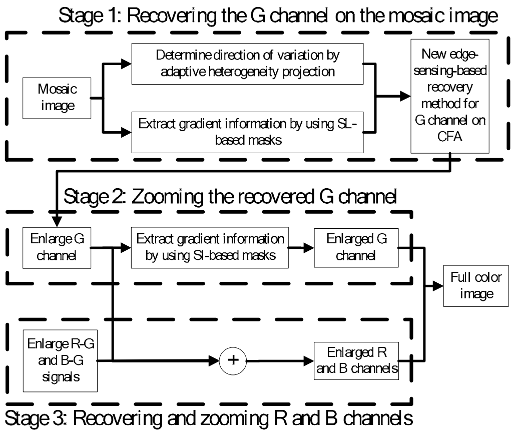

Fig. 2. The detailed flowchart of the proposed joint demosaicing and zooming algorithm.

image zooming method proposed by Lukac *et al.* [17] with the demosaicing method proposed by Zhang and Wu [28]; the algorithm combining one of the two demosaicing methods proposed by Lukac *et al.* [14] and Zhang and Wu [28], respectively, with the bilinear image zooming method, and two recently published algorithms, one by Chung and Chan [5] and the other by Zhang and Zhang [30].

The remainder of this paper is organized as follows. In Section II, we describe how to extract more accurate edge information of each pixel directly from the mosaic image. In Section III, our proposed joint demosaicing and zooming algorithm is presented. In Section IV, some experimental results are demonstrated to carry out the quality advantages of our proposed algorithm. Finally, some concluding remarks are addressed in Section V.

II. EXTRACTING EDGE INFORMATION ON MOSAIC IMAGES

Before presenting our proposed new joint demosaicing and zooming algorithm for mosaic images, this section introduces how to generate heterogeneity projection map adaptively and how to extract more accurate edge information of each pixel based on the SL-based masks. The generated heterogeneity projection map and extracted more accurate edge information will be used in our proposed new joint demosaicing and zooming algorithm in Section III. Throughout the paper, $I^r_{mo}(i,j)$, $I^g_{mo}(i,j)$, and $I^b_{mo}(i,j)$ denote R, G, and B pixels at position (i,j) on the mosaic image I_{mo}; $I^g_{dm}(i,j)$ denotes the demosaiced G pixel at position (i,j); the R, G, and B values of the zoomed full color image I^z_{dm} at position (i,j) are denoted by $I^{z,r}_{dm}(i,j)$, $I^{z,g}_{dm}(i,j)$, and $I^{z,b}_{dm}(i,j)$, respectively.

A. Adaptive heterogeneity projection for mosaic images

In this subsection, the adaptive heterogeneity projection [7] for mosaic images is described. Based on the concept of adaptive heterogeneity projection, the three possible heterogeneity projection masks with different sizes adopted in this paper are shown in Table I. In Table I, the terms N and $M_{hp}(N)$ denote the mask size and the corresponding heterogeneity projection mask, respectively. Given a mosaic image I_{mo}, we can generate the horizontal heterogeneity

TABLE I.
FOUR POSSIBLE HETEROGENEITY PROJECTION MASKS.

N	$M_{hp}(N)$
5	$[1\ \ -2\ \ 0\ \ 2\ \ 1]$
7	$[1\ \ -4\ \ 5\ \ 0\ \ -5\ \ 4\ \ -1]$
9	$[1\ \ -6\ \ 14\ \ -14\ \ 0\ \ 14\ \ -14\ \ 6\ \ -1]$

projection map HP_{H-map} and the vertical heterogeneity projection map HP_{V-map} by

$$HP_{H-map} = | I_{mo} \otimes M_{hp}(N)^T |$$

$$HP_{V-map} = | I_{mo} \otimes M_{hp}(N) |$$

where the symbol "$\otimes$" denotes the 1-D convolution operator; $|\cdot|$ denotes the absolute value operator and the operator "T" denotes the transpose operator. The readers are suggested to refer [7] for understanding the detailed explanation on the determination of N and $M_{hp}(N)$. For exposition, the determined proper horizontal heterogeneity projection mask size N is called N_H.

After determining the proper mask size N_H, the proper heterogeneity projection mask can be easily obtained from Table I. In order to normalize the masks with different sizes, we use the normalization factor $\frac{1}{Q_{(N_H)}}$ to normalize the coefficients of the mask where the value of $Q_{(N_H)}$ is defined as the sum of positive coefficients covered by the mask with size N_H. For example, if $N_H = 5$, the value of $Q_{(5)}$ is 3, and the heterogeneity projection mask $[1\ \ -2\ \ 0\ \ 2\ \ -1]^T$ would be normalized to $\frac{[1\ \ -2\ \ 0\ \ 2\ \ -1]^T}{3}$.

In order to reduce the estimation error, we use the low-pass filter to tune the heterogeneity projection maps. For HP_{H-map} and HP_{V-map}, the horizontal and vertical heterogeneity projection values at location (i,j) are denoted by $HP_H(i,j)$ and $HP_V(i,j)$, respectively. The following two low-pass filters $HP'_H(i,j) = \sum_{k=-4}^{4} \delta_k HP_H(i,j+k)$ and $HP'_V(i,j) = \sum_{k=-4}^{4} \delta_k HP_V(i+k,j)$ where $\delta_k = 2$ if $k=0$; $\delta_k = 1$, otherwise, could be used to compute the tuned horizontal and vertical heterogeneity projection values, $HP'_H(i,j)$ and $HP'_V(i,j)$.

B. Sobel- and luminance estimation-based (SL-based) masks for G channel on mosaic images

In this subsection, the approach to extract gradient information for the G channel on mosaic images directly and accurately is introduced. In order to extract more accurate edge information from mosaic images, the luminance estimation technique [1] is embedded into the Sobel operator [8]. The detailed derivations of embedding the luminance estimation technique into the Sobel

Authorized licensed use limited to: National Taiwan Univ of Science and Technology. Downloaded on October 13, 2009 at 22:45 from IEEE Xplore. Restrictions apply.

-1	-2	0	2	1
-4	-8	0	8	4
-6	-12	0	12	6
-4	-8	0	8	4
-1	-2	0	2	1

(a)

-1	-4	-6	-4	-1
-2	-8	-12	-8	-2
0	0	0	0	0
2	8	12	8	2
1	4	6	4	1

(b)

Fig. 3. The two SL-based masks. (a) The horizontal SL-based mask. (b) The vertical SL-based mask.

operator are described in [7]. For avoiding the floating point computation, the coefficients in the masks are normalized into integers in advance and the two normalized SL-based masks are shown in Fig. 3. After running the proper SL-based masks on the 5×5 mosaic subimage centered at position (i,j), the horizontal response $\Delta I_{dm}^{H}(i,j)$ and the vertical response $\Delta I_{dm}^{V}(i,j)$ of G channel can be obtained.

By examining the horizontal SL-based mask and the vertical SL-based mask as shown in Fig. 3(a) and Fig. 3(b), respectively, for each mask, it is observed that only five numbers, 2, 4, 6, 8, and 12, are used. This observation leads to a faster way to run the mask on the mosaic subimage and it needs only five multiplications, nineteen additions, and ten absolute-value operation rather than twenty multiplications, nineteen additions, and ten absolute-value operations.

III. The Proposed Joint Demosaicing and Zooming Algorithm

In this section, based on the extracted edge information mentioned in Section II, our proposed new joint demosaicing and zooming algorithm is presented in detail. In our proposed algorithm, the whole process consists of the following three stages: (1) recovering the G channel to obtain the complete G channel I_{dm}^{g} by using the edge-sensing demosaicing algorithm; (2) zooming the recovered complete G channel I_{dm}^{g} to obtain the zoomed G channel $I_{dm}^{z,g}$; (3) recovering and zooming R and B channels by using the color difference value to obtain the zoomed R channel $I_{dm}^{z,r}$ and B channel $I_{dm}^{z,b}$, and finally the zoomed full color image can be obtained. The flowchart of the three stages in our proposed joint demosaicing and zooming algorithm is shown in Fig. 2.

A. Recovering the G channel on the mosaic image

In this subsection, the G channel recovery on the mosaic image by using the extracted edge information mentioned in Section II and the edge-sensing demosaicing algorithm are presented. For exposition, let us take Fig. 1 to explain how to estimate the G channel value $I_{dm}^{g}(i,j)$ located at the center position of Fig. 1. In order to estimate $I_{dm}^{g}(i,j)$ more accurately by using its four neighboring pixels with movement $\Omega_n=\{(x,y)|(x,y)=(i\pm 1,j),(i,j\pm 1)\}$, four proper weights in terms of the gradient magnitude are assigned to the corresponding four spectral-correlation terms in the interpolation estimation phase. Considering the neighboring pixel located at position $(i-1,j)$, if the vertical gradient magnitude of the pixel at position $(i-1,j)$ is large, it means that there is a horizontal edge passing through it. Based on the color difference assumption [13], [23], it reveals that the G component of this pixel makes less contribution to the estimation of the G component of the current pixel at position (i,j); otherwise, it reveals that the G component of this pixel makes more contribution to the estimation of the G component of the current pixel. Based on the above analysis of gradient and direction influences, the weight of the pixel at position $(i-1,j)$ can be determined by $w_g(V,i-1,j)=\dfrac{1}{1+\Delta I_{dm}^{V}(i,j)+2\Delta I_{dm}^{V}(i-1,j)+\Delta I_{dm}^{V}(i-2,j)}$. By the same argument, the weights of the other three neighbors of the current pixel can be determined by $w_g(V,i+1,j)=\dfrac{1}{1+\sum_{k=0}^{2}\delta_k\Delta I_{dm}^{V}(i+k,j)}$, $w_g(H,i,j-1)=\dfrac{1}{1+\sum_{k=0}^{2}\delta_k\Delta I_{dm}^{H}(i,j-k)}$, and $w_g(H,i,j+1)=\dfrac{1}{1+\sum_{k=0}^{2}\delta_k\Delta I_{dm}^{H}(i,j+k)}$, respectively where $\delta_k=2$ if $k=1$; $\delta_k=1$, otherwise. In addition, based on the horizontal and vertical heterogeneity projection values of the current pixel at position (i,j), $HP_H^{'}(i,j)$ and $HP_V^{'}(i,j)$, the interpolation estimation scheme for G channel should consider three cases, namely (1) horizontal variation (HV) as shown in Fig. 4(a), (2) vertical variation (VV) as shown in Fig. 4(b), and (3) the other variations (OV) as shown in Fig. 4(c). The arrows in Fig. 4 denote the relevant data dependence.

According to the above discussions, the value of $I_{dm}^{g}(i,j)$ can be estimated by the following rule:

$$I_{dm}^{g}(i,j)=I_{mo}^{b}(i,j)+\frac{\sum_{(d,x,y)\in\xi_g} w_g(d,x,y)D_g(x,y)}{\sum_{(d,x,y)\in\xi_g} w_g(d,x,y)}$$

$$\xi_g=\begin{cases}\xi_1 & \text{if } DVar(i,j)=H\\ \xi_2 & \text{if } DVar(i,j)=V\\ \xi_1\cup\xi_2 & \text{if } DVar(i,j)=O\end{cases}$$

$$DVar(i,j)=\begin{cases}H\ (\text{HV}) & \text{if } HP_V^{'}(i,j)<\alpha HP_H^{'}(i,j)\\ V\ (\text{VV}) & \text{if } HP_H^{'}(i,j)<\alpha HP_V^{'}(i,j)\\ O\ (\text{OV}) & \text{Ohterwise}\end{cases}$$

where $\xi_1=\{(V,i\pm 1,j)\}$ and $\xi_2=\{(H,i,j\pm 1)\}$; for $(d,x,y)\in\xi_1$, $D_g(x_1,y_1)=I_{mo}^{g}(x_1,y_2)-\dfrac{I_{mo}^{b}(x_1+1,y_2)+I_{mo}^{b}(x_1-1,y_2)}{2}$; for $(d,x,y)\in\xi_1$, $D_g(x_1,y_1)=I_{mo}^{g}(x_1,y_2)-\dfrac{I_{mo}^{b}(x_1+1,y_2)+I_{mo}^{b}(x_1-1,y_2)}{2}$;

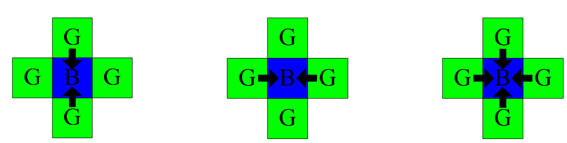

(a) (b) (c)

Fig. 4. Data dependence of our proposed interpolation estimation for G channel. (a) Horizontal variation (vertical edge). (b) Vertical variation (horizontal edge). (c) The other variations.

Authorized licensed use limited to: National Taiwan Univ of Science and Technology. Downloaded on October 13, 2009 at 22:45 from IEEE Xplore. Restrictions apply.

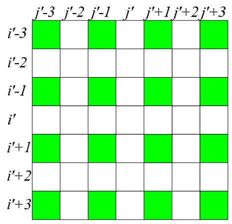

Fig. 5. The pattern of $I_{dm}^{z,g}$ after expanding the recovered G channel.

$DVar(i,j)$ denotes the direction of variation at position (i,j); the parameter α is set to $\alpha = 0.55$ empirically.

After recovering the G channel by using the above rules, the proposed new refinement method, which combines the concept of the local color ratios [16] and our proposed proper weighting scheme based on the gradient magnitude, is used to refine the demosaiced G channel. For the pixel at position (i,j), its G color value $I_{dm}^{g}(i,j)$ is refined by

$$I_{dm}^{g}(i,j) = -\beta + (I_{mo}^{b}(i,j)+\beta)\frac{\sum_{(d,x,y)\in\xi_g^{'}}\delta_{(d,x,y)}w_g(d,x,y)L_g(x,y)}{\sum_{(d,x,y)\in\xi_g^{'}}\delta_{(d,x,y)}w_g(d,x,y)}$$

where $\xi_g^{'} = \{(H,i,j),(V,i,j),(H,i,j\pm1),(V,i\pm1,j)\}$; $L_g(x,y) = \frac{I_{dm}^{g}(x,y)+\beta}{I_{mo}^{b}(x,y)+\beta}$; $\delta_{(d,x,y)} = 0.5$ if $(d,x,y) = \{(H,i,j),(V,i,j)\}$; $\delta_{(d,x,y)} = 1$, otherwise; the parameter β is set to $\beta = 256$ empirically. In next subsection, the recovered G channel will be used to estimate the G color values of the zoomed full color image.

B. Zooming the recovered G channel

After recovering the G channel on the mosaic image, in this subsection, we present an efficient method to zoom the recovered G channel and the zoomed G channel is called $I_{dm}^{z,g}$. If the recovered G channel I_{dm}^{g} is with size $X \times Y$, after the quad-zooming process, the size of the obtained zoomed G channel $I_{dm}^{z,g}$ is $2X \times 2Y$. In order to obtain the zoomed G channel $I_{dm}^{z,g}$, the recovered green channel I_{dm}^{g} is first expanded to $I_{dm}^{z,g}$ and the array $DVar$, which has saved the directions of variation of all pixels in I_{dm}^{g}, is expanded to $DVar^{z}$; the expanding rule is given by

$$I_{dm}^{z,g}(2i,2j) = I_{dm}^{g}(i,j);\ DVar^{z}(2i,2j) = DVar(i,j),$$
$$\forall i \in \{0,1,2,\ldots,X-1\};\ \forall j \in \{0,1,2,\ldots,Y-1\}$$

where $DVar^{z}(x,y)$ denotes the direction of variation at position (x,y) in the zoomed green channel $I_{dm}^{z,g}$. After expanding the recovered G channel by using the above rule, the pattern of $I_{dm}^{z,g}$ is now illustrated in Fig. 5. The interpolation estimation for G channel could be partitioned into two steps: Step 1: interpolating the G values of pixels at positions $(i'+2m, j'+2n)$ in Fig. 5; Step 2: interpolating the missing G values of pixels at positions $(i'+2m, j'+2n+1)$ and $(i'+2m+1, j'+2n)$.

For simplicity, we now take the central pixel at position (i',j') as the representative to explain how to estimate the G values in Step 1. Step 2 will be described later. Referring to Fig. 5, it is not hard to find that the G pattern in Fig. 5 is the same as the R/B pattern in the mosaic image as shown in Fig. 1. According to [7], the R/B gradient information of the mosaic image can be extracted by using the four quad-masks which combine the bilinear interpolation demosaicing technique and the Sobel operator; the required four quad-masks are shown in Fig. 6–Fig. 9. Because of the equivalence of the two patterns mentioned above, the gradient magnitudes of all pixels in $I_{dm}^{z,g}$ (see Fig. 5) can also be extracted by using the four quad-masks as shown in Fig. 6–Fig. 9. By running the proper SI-based masks on the 5×5 subimage centered at position (i',j') in Fig. 5, the horizontal response $\Delta I_{dm}^{z,H}(i',j')$, the vertical response $\Delta I_{dm}^{z,V}(i',j')$, the $\pi/4$-diagonal response $\Delta I_{dm}^{z,\pi/4}(i',j')$, and the $-\pi/4$-diagonal response $\Delta I_{dm}^{z,-\pi/4}(i',j')$ of G channel can be obtained.

Similar to the recovering process for the mosaic G channel mentioned in last subsection, assume the gradient magnitudes of the current pixel at position (i',j') and the four neighboring pixels with movement $\Omega_n^{'} = \{(x,y)\,|\,(x,y) = (i'\pm1, j'\pm1)\}$, respectively, have been computed by the above rule. In order to estimate the G value of the current pixel $I_{dm}^{z,g}(i',j')$ more accurately, the gradient magnitudes of four diagonal variations are considered to determine the proper four weights. Similar to the analysis in last subsection, the four weights of the four diagonal neighbors of the current pixel can be given by

$$w_g^{z}(-\pi/4, i'-1, j'-1) = \frac{1}{1+\sum_{k=0}^{2}\delta_k \Delta I_{dm}^{z,-\pi/4}(i'-k, j'-k)},$$

$$w_g^{z}(\pi/4, i'-1, j'+1) = \frac{1}{1+\sum_{k=0}^{2}\delta_k \Delta I_{dm}^{z,\pi/4}(i'-k, j'+k)},$$

$$w_g^{z}(\pi/4, i'+1, j'-1) = \frac{1}{1+\sum_{k=0}^{2}\delta_k \Delta I_{dm}^{z,\pi/4}(i'+k, j'-k)},$$

and

$$w_g^{z}(-\pi/4, i'+1, j'+1) = \frac{1}{1+\sum_{k=0}^{2}\delta_k \Delta I_{dm}^{z,-\pi/4}(i'+k, j'+k)},$$

where $\delta_k = 2$ if $k = 1$; $\delta_k = 2$, otherwise. Based on the four weights, the G value of the current pixel at position (i',j') can be estimated by

$$I_{dm}^{z,g}(i,j) = \frac{\sum_{(d,x,y)\in\xi_g^{z'}} w_g^{z}(d,x,y) I_{dm}^{z,g}(x,y)}{\sum_{(d,x,y)\in\xi_g^{z'}} w_g^{z}(d,x,y)}$$

where $\xi_g^{z'} = \{(-\pi/4, i'-1, j'-1), (\pi/4, i'-1, j'+1), (\pi/4, i'+1, j'-1), (-\pi/4, i'+1, j'+1)\}$. Furthermore, at position (i',j'), the direction of variation $DVar^{z}(i',j')$ can be determined by the following rule:

$$DVar^{z}(i',j') = \begin{cases} H\ \text{(HV)} & \text{if} \sum_{(x,y)\in\Omega_n^{'}} NVar^{z}(x,y) \ge 2 \\ V\ \text{(VV)} & \text{if} \sum_{(x,y)\in\Omega_n^{'}} NVar^{z}(x,y) \le -2 \\ O\ \text{(OV)} & \text{otherwise} \end{cases}$$

$$NVar^{z}(x',y') = \begin{cases} 1 & \text{if } DVar^{z}(x',y') = H \\ -1 & \text{if } DVar^{z}(x',y') = V \\ 0 & \text{otherwise} \end{cases} \quad (1)$$

Authorized licensed use limited to: National Taiwan Univ of Science and Technology. Downloaded on October 13, 2009 at 22:45 from IEEE Xplore. Restrictions apply.

where $\Omega'_n = \{(x,y) | (x,y) = (i'\pm 1, j'\pm 1)\}$; for all $(x', y') \in \Omega'_n$. The determined $DVar^z(i', j')$ will be used in Step 2 later.

After performing Step 1, Fig. 10(a) illustrates the current pattern of the zoomed G channel. For easy exposition for recovering missing G pixels, instead of using Fig. 10(a), Fig. 10(b) (which is obtained by shifting Fig. 10(a) one pixel down, i.e. the position (i'', j'') in Fig. 10(b) corresponds to the position $(i'-1, j')$ in Fig. 10(a)) is used. For simplicity, we still take the central pixel at position (i'', j'') as the representative to explain how to estimate the missing G values which constitutes the main body of Step 2.

Referring to Fig. 10(b), since the G pattern of the zoomed G channel $I^{z,g}_{dm}$ is the same as that of the mosaic image, the interpolation estimation approach mentioned in Subsection III.A can be used to estimate the G value of the current pixel

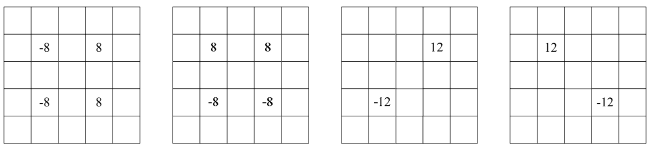

(a) (b) (c) (d)

Fig. 6. For all $(x,y) \in \{(i'\pm 2m, j'\pm 2n)\}$ in Fig. 5, the four SI-based masks for G channel. (a) The horizontal SI-based mask. (b) The vertical SI-based mask. (c) The $\pi/4$-diagonal SI-based mask. (d) The $-\pi/4$-diagonal SI-based mask.

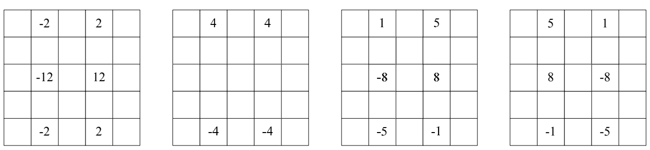

(a) (b) (c) (d)

Fig. 7. For all $(x,y) \in \{(i'\pm 2m+1, j'\pm 2n)\}$ in Fig. 5, the four SI-based masks for G channel. (a) The horizontal SI-based mask. (b) The vertical SI-based mask. (c) The $\pi/4$-diagonal SI-based mask. (d) The $-\pi/4$-diagonal SI-based mask.

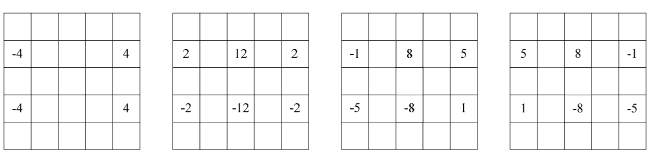

(a) (b) (c) (d)

Fig. 8. For all $(x,y) \in \{(i'\pm 2m, j'\pm 2n+1)\}$ in Fig. 5, the four SI-based masks for G channel. (a) The horizontal SI-based mask. (b) The vertical SI-based mask. (c) The $\pi/4$-diagonal SI-based mask. (d) The $-\pi/4$-diagonal SI-based mask.

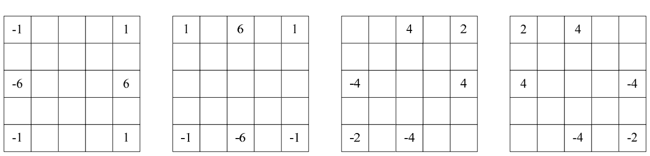

(a) (b) (c) (d)

Fig. 9. For all $(x,y) \in \{(i'\pm 2m+1, j'\pm 2n+1)\}$ in Fig. 5, the four SI-based masks for G channel. (a) The horizontal SI-based mask. (b) The vertical SI-based mask. (c) The $\pi/4$-diagonal SI-based mask. (d) The $-\pi/4$-diagonal SI-based mask.

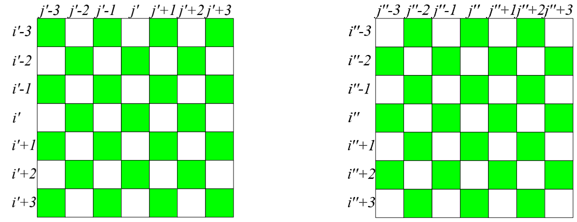

(a) (b)

Fig. 10. Two patterns of the zoomed G channel. (a) The pattern of the zoomed G channel after performing Step 1. (b) The pattern shifting (a) one pixel down.

at position (i'', j''). Similar to Eq. (1), the direction of variation $DVar^z(i'', j'')$ is first determined by considering its four neighboring pixels with movement $\Omega''_n = \{(x,y) | (x,y) = (i''\pm 1, j), (i'', j\pm 1)\}$. After determining the direction of variation $DVar^z(i'', j'')$, the G value of the current pixel at position (i'', j'') can be estimated by

$$I^{z,g}_{dm}(i'', j'') = \frac{\sum_{(d,x,y)\in\xi^{z''}_g} w^z_g(d,x,y) I^{z,g}_{dm}(x,y)}{\sum_{(d,x,y)\in\xi^{z''}_g} w^z_g(d,x,y)}$$

$$\xi''_g = \begin{cases} \xi_1 & \text{if } DVar^z(i'', j'') = H \\ \xi_2 & \text{if } DVar^z(i'', j'') = V \\ \xi_1 \cup \xi_2 & \text{if } DVar^z(i'', j'') = O \end{cases}$$

where $\xi_1 = \{(V, i''\pm 1, j'')\}$ and $\xi_2 = \{(H, i'', j''\pm 1)\}$; $DVar^z(i'', j'')$ denotes the direction of variation at position (i'', j''); $w_g(V, i''-1, j'') = \frac{1}{1+\sum_{k=0}^{2} \delta_k \Delta I^{z,V}_{dm}(i''-k, j'')}$;

$w_g(V, i''+1, j'') = \frac{1}{1+\sum_{k=0}^{2} \delta_k \Delta I^{z,V}_{dm}(i''+k, j'')}$;

$w_g(H, i'', j''-1) = \frac{1}{1+\sum_{k=0}^{2} \delta_k \Delta I^{z,H}_{dm}(i'', j''-k)}$;

$w_g(H, i'', j''+1) = \frac{1}{1+\sum_{k=0}^{2} \delta_k \Delta I^{z,H}_{dm}(i'', j''+k)}$; $\delta_k = 2$ if $k = 1$; $\delta_k = 2$, otherwise.

After performing the above interpolation estimation for G pixels, the G channel of the zoomed image has been fully populated. In next subsection, the fully populated G channel of the zoomed image will be used to assist the interpolation estimation of R and B channels.

C. Recovering and zooming R and B channels

Since the G channel is completely recovered and zoomed, the color difference concept can be used to assist the recovery of R and B pixels more accurately. Instead of demosaicing R and B channels of the mosaic image in Fig. 1, R and B pixels on the mosaic image are directly expanded to the zoomed R channel $I^{z,r}_{dm}$ and the zoomed B channel $I^{z,b}_{dm}$, respectively, by using the rule:

$$\begin{aligned} I^{z,r}_{dm}(2i_r, 2j_r) &= I^r_{mo}(i_r, j_r) \\ I^{z,b}_{dm}(2i_b, 2j_b) &= I^b_{mo}(i_b, j_b) \end{aligned} \quad (2)$$

Authorized licensed use limited to: National Taiwan Univ of Science and Technology. Downloaded on October 13, 2009 at 22:45 from IEEE Xplore. Restrictions apply.

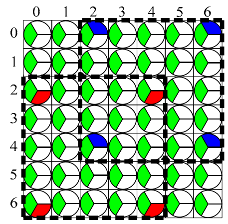

Fig. 11. The subimage of I_{dm}^{z} after expanding R and B channels.

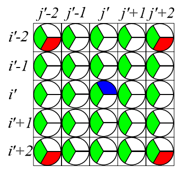

Fig. 12. A basic block.

where $I_{mo}^{r}(i_r, j_r)$ denotes the R pixel at position (i_r, j_r) in the mosaic image I_{mo}; $I_{mo}^{b}(i_b, j_b)$ denotes the B pixel at position (i_b, j_b) in I_{mo}; $I_{dm}^{z,r}(x,y)$ and $I_{dm}^{z,b}(x,y)$ denote the R and B color values of the zoomed image I_{dm}^{z} at position (x,y), respectively. For example, by Eq. (2), the R pixel at position $(1,0)$ in the mosaic image I_{mo} is copied to position $(2,0)$ in the zoomed image I_{dm}^{z} as shown in Fig. 11. In order to cover the four copied R pixels in Fig. 11, a basic 5×5 block surrounded by dashed lines is used to recover the missing R pixels. It is followed for the four copied B pixels. Since the recovering and zooming approach for R channel is the same as that for B channel, in what follows, we only present it for R channel.

Fig. 12 illustrates a basic block which is cut off from Fig. 11. It is observed that the four corner pixels of the basic block contain R and G values simultaneously. Thus, color difference values of the four corner pixels can be first obtained by $D_r^z(x,y) = I_{dm}^{z,g}(x,y) - I_{dm}^{z,r}(x,y), \quad \forall (x,y) \in \{(i'\pm 2, j'\pm 2)\}$. Then, according to the concept of bilinear interpolation estimation, the missing color difference values in the basic block could be obtained by

$$D_r^z(i'+m, j'+n) = \sum_{\delta_1} \frac{2+\delta_1 n}{4} \sum_{\delta_2} \frac{2+\delta_2 m}{4} D_r^z(i'+2\delta_2, j'+2\delta_1)$$

where $\delta_1, \delta_2 \in \{-1,1\}$; $-2 \le m,n \le 2$. In order to speed up the computation of $D_r^z(i'+m, j'+n)$, based on the derivation in [6], the above equation can be rewritten by

$$D_r^z(i'+m, j'+n) = D_r^z(i'-2, j'-2) + \frac{m+2}{4}\Delta D_r^{z,V} + \frac{n+2}{4}\Delta D_r^{z,H} + \frac{(m+2)(n+2)}{16}F_1$$

where $0 \le m+2, n+2 \le 4$; $\Delta D_r^{z,V} = \sum_{s\in\{-1,1\}} sD_r^z(i'+2s, j'-2)$; $\Delta D_r^{z,H} = \sum_{s\in\{-1,1\}} sD_r^z(i'-2, j'+2s)$; $F_1 = \sum_k \sum_l \delta_{k,l} D_r^z(i'+2k, j'+2l)$ where $k,l \in \{-1,1\}$; $\delta_{k,l} = kl$. It is observed that in Eq. **Error! Reference source not found.** for each basic block, $\Delta D_r^{z,V}$, $\Delta D_r^{z,H}$, and F_1 should be only calculated once. After getting color difference values for all pixels in the basic block, all the missing R color values in the basic block can be recovered by

Fig. 13. The twenty-four testing images from Kodak PhotoCD [31].

$I_{dm}^{z,r}(i'+m, j'+n) = I_{dm}^{z,g}(i'+m, j'+n) - D_r^z(i'+m, j'+n)$ where $-2 \le m,n \le 2$.

After presenting our proposed new joint demosaicing and zooming algorithm, in next section, some experimental results are shown to demonstrate the quality advantage of our proposed algorithm.

IV. EXPERIMENTAL RESULTS

In this section, based on twenty-four testing mosaic images, some experimental results are demonstrated to show that our proposed joint demosaicing and zooming algorithm has better image quality performance when compared with the previous zooming algorithms. Fig. 13 illustrates the twenty-four testing images from Kodak PhotoCD [31]. In our experiments, the twenty-four testing images with size 512×728 are first down-sampled to obtain the mosaic images with size 256×364. Furthermore, the boundaries of the image are dealt with using the mirroring method.

For evaluating the performance of our proposed zooming algorithm, five zooming algorithms for mosaic images are used to compare with our proposed algorithm. In the first comparative algorithm called A_1, the zoomed mosaic images are first produced by using the mosaic image zooming algorithm proposed by Lukac *et al.* [17] and then the demosaicing method proposed by Zhang and Wu [28] is used to demosaic the zoomed mosaic image. In [5], the bilinear image zooming [26] method is a good choice to zoom the demosaiced images. In the second and third comparative algorithm A_2 and A_3, the two demosaicing methods proposed by Lukac *et al.* [14] and Zhang and Wu [28] are first used to obtain the demosaiced images and then the bilinear image zooming method is used to produce the zoomed full color images. Considering the fourth and fifth comparative algorithm, A_4 and A_5, two recently published joint demosaicing and zooming algorithms, one by Chung and Chan [6] and the other by Zhang and Zhang [30], are used to zoom the mosaic images. The concerned algorithms are implemented on the IBM compatible computer with Intel Core 2 Duo CPU 1.83GHz and 2GB RAM. The operating system used is MS-Windows XP and the program developing environment is Dev C++ 4.9.9.2. Our implementations for the concerned algorithms and the concerned results are available from [32].

Authorized licensed use limited to: National Taiwan Univ of Science and Technology. Downloaded on October 13, 2009 at 22:45 from IEEE Xplore. Restrictions apply.

TABLE II.
THE CPSNR QUALITY COMPARISON.

	A_1	A_2	A_3	A_4	A_5	*Ours*
Image01	22.80	24.15	24.59	24.46	24.37	**24.68**
Image02	29.26	30.62	30.54	30.41	30.60	**30.91**
Image03	30.41	32.04	31.94	32.10	32.06	**32.55**
Image04	28.92	31.07	31.07	30.91	31.13	**31.40**
Image05	22.20	24.37	24.65	24.59	24.71	**24.91**
Image06	24.22	25.49	26.28	26.03	26.01	**26.39**
Image07	28.48	31.05	30.83	30.75	31.31	**31.50**
Image08	20.12	21.45	21.92	21.76	21.74	**22.12**
Image09	28.44	30.15	30.46	30.31	30.63	**30.88**
Image10	28.36	30.23	30.55	30.49	30.59	**30.86**
Image11	25.50	27.00	27.36	27.21	27.24	**27.61**
Image12	29.74	31.19	31.40	31.41	31.43	**31.80**
Image13	20.36	21.91	22.43	22.22	22.15	**22.55**
Image14	24.69	26.50	26.26	26.22	26.33	**26.68**
Image15	28.74	30.57	30.50	30.60	30.72	**31.07**
Image16	27.85	29.04	29.70	29.55	29.46	**29.84**
Image17	28.14	30.14	30.48	30.18	30.46	**30.77**
Image18	24.11	25.88	26.20	26.00	26.05	**26.43**
Image19	24.47	2570	26.47	26.19	26.36	**26.63**
Image20	27.76	29.45	29.68	29.72	29.80	**30.10**
Image21	24.72	26.26	26.71	26.52	26.53	**26.91**
Image22	26.45	28.00	28.10	27.89	28.03	**28.42**
Image23	29.67	32.11	32.09	32.23	32.52	**32.57**
Image24	22.84	24.46	24.97	24.71	24.78	**25.08**
Average	26.18	27.87	28.14	28.02	28.13	**28.44**

TABLE III.
THE S-CIELAB ΔE^*_{ab} QUALITY COMPARISON.

	A_1	A_2	A_3	A_4	A_5	*Ours*
Image01	5.788	5.099	4.462	4.398	4.719	**4.052**
Image02	3.922	3.454	3.434	3.652	3.484	**3.177**
Image03	2.457	2.055	2.158	2.087	2.134	**1.958**
Image04	3.481	2.925	2.831	2.888	2.853	**2.666**
Image05	8.042	6.765	6.510	6.462	6.763	**5.925**
Image06	4.162	3.722	2.950	3.069	3.157	**2.844**
Image07	3.602	2.641	2.903	2.711	2.687	**2.523**
Image08	6.546	5.718	4.841	4.748	5.031	**4.470**
Image09	2.373	1.978	1.865	1.860	1.829	**1.702**
Image10	2.335	2.004	1.887	1.884	1.886	**1.734**
Image11	4.462	3.850	3.514	3.528	3.670	**3.241**
Image12	1.887	1.607	1.533	1.487	1.534	**1.400**
Image13	8.053	7.179	6.090	6.504	6.661	**5.861**
Image14	5.608	4.736	4.728	4.725	4.856	**4.379**
Image15	3.521	3.083	3.095	3.038	3.094	**2.840**
Image16	3.212	2.888	2.292	2.356	2.422	**2.218**
Image17	3.650	3.000	2.768	2.878	2.884	**2.644**
Image18	6.557	5.638	5.485	5.544	5.669	**5.084**
Image19	4.071	3.519	2.982	3.125	3.150	**2.824**
Image20	2.776	2.332	2.275	2.232	2.332	**2.079**
Image21	4.151	3.605	3.155	3.259	3.376	**2.987**
Image22	3.854	3.381	3.411	3.423	3.397	**3.145**
Image23	2.393	**1.909**	2.193	1.996	2.029	1.981
Image24	4.580	3.988	3.603	3.758	3.766	**3.362**
Average	4.229	3.626	3.374	3.400	3.474	**3.129**

Here, two objective color image quality measures, the color PSNR (CPSNR) and the S-CIELAB ΔE^*_{ab} metric [10], [13], and one subjective color image quality measure, the color artifacts, are adopted to justify the better quality performance of our proposed novel zooming algorithm. The CPSNR for a color image with size $M \times N$ is defined by

$$\text{CPSNR}=10\log_{10}\frac{255^2}{\frac{1}{3MN}\sum_{i=0}^{M-1}\sum_{j=0}^{N-1}\sum_{c\in C}\left[I^c_{ori}(i,j)-I^{z,c}_{dm}(i,j)\right]^2}$$

where $C \in \{r,g,b\}$; $I^r_{ori}(i,j)$, $I^g_{ori}(i,j)$, and $I^b_{ori}(i,j)$ denote the three color components of the color pixel at position (i,j) in the original full color image; $I^{z,r}_{dm}(i,j)$, $I^{z,g}_{dm}(i,j)$, and $I^{z,b}_{dm}(i,j)$ denote the three color components of the color pixel at position (i,j) in the zoomed full color image. The greater the CPSNR is, the better the image quality is. The S-CIELAB ΔE^*_{ab} of a color image with size $M \times N$ is defined by

$$\Delta E^*_{ab} = \frac{1}{MN}\sum_{i=0}^{M-1}\sum_{j=0}^{N-1}\left\{\sqrt{\sum_{c\in\Psi} LAB^c_{ori}(i,j)-LAB^{z,c}_{dm}(i,j)}\right\}$$

where $\Psi \in \{L,a,b\}$; $LAB^L_{ori}(i,j)$, $LAB^a_{ori}(i,j)$, and $LAB^b_{ori}(i,j)$ denote the three CIELAB color components of the color pixel at position (i,j) in the original full color image; $LAB^{z,L}_{dm}(i,j)$, $LAB^{z,a}_{dm}(i,j)$, and $LAB^{z,b}_{dm}(i,j)$ denote the three CIELAB color components of the color pixel at position (i,j) in the zoomed full color image. The smaller the S-CIELAB ΔE^*_{ab} is, the better the image quality is.

For fairness, the recently published joint demosaicing and zooming algorithms [5], [30] still apply their own demosaiced image quality refinement schemes; the two demosaicing methods [14], [28] also utilize the postprocessing approach by Lukac *et al.* [16] to enhance the demosaiced image quality. Based on twenty-four testing images, among our proposed zooming algorithm and the other five zooming algorithms, Table II and Table III demonstrate the zoomed image quality comparison in terms of CPSNR and S-CIELAB ΔE^*_{ab}, respectively. In Table II and Table III, the entries with the largest CPSNR and the smallest S-CIELAB ΔE^*_{ab}, respectively, are highlighted by boldface. In average, our proposed zooming algorithm has the best zoomed image quality in terms of CPSNR and S-CIELAB ΔE^*_{ab} among the concerned six zooming algorithms.

Then, the subjective image visual measure is adopted to demonstrate the visual quality advantage of our proposed zooming algorithm. After recovering and zooming the mosaic image, some color artifacts may appear on nonsmooth regions of the zoomed full color image. Here, seven magnified subimages cut from the testing image No. 5 are used to compare the visual effect among the six concerned algorithms. Fig. 14(a)–Fig. 14(g) illustrate the magnified subimages cut from the original testing image No. 5 and the ones obtained by the six concerned zooming algorithms. Comparing the visual effect between each magnified subimage in Fig. 14(a) and the corresponding one in Fig. 14(b)–Fig. 14(g), it is observed that our proposed zooming algorithm produces less color artifacts when compared to the other five previous zooming algorithms. Further, we take the magnified subimages cut from the testing

Authorized licensed use limited to: National Taiwan Univ of Science and Technology. Downloaded on October 13, 2009 at 22:45 from IEEE Xplore. Restrictions apply.

TABLE IV.
AVERAGE NUMBERS OF OPERATIONS REQUIRED FOR DEMOSAICING AND ZOOMING A PIXEL REQUIRED IN OUR PROPOSED ALGORITHM.

	ADD	MUL	DIV	CMP	ABS
Stage 1: Recovering the G channel on the mosaic image.					
Determine direction of variation by adaptive heterogeneity projection.	38	5.333	4	12	8
Extract G channel gradient information on the mosaic image by SL-based masks.	38	10	0	0	20
Recover the G channel on the mosaic image by edge-sensing interpolation.	20	5	6.5	0.5	0
Stage 2: Zooming the recovered G channel.					
Extract gradient information on the expanded G channel by SI-based masks.	16	6	0	0	10
Interpolate the G color values.	13.25	5	3.25	0.75	0
Stage 3: Recovering and zooming the R and B channels.					
Interpolate the R and B color values.	10.125	5.625	5.625	0	0
Number of total generations.	135.375	36.958	19.375	13.25	38

image No. 19 for visual comparison. Fig. 15(a)–Fig. 15(g) are the magnified subimages cut from the original full color testing image No. 19 and the six zoomed images. From visual comparison, it is observed that among the six concerned zooming algorithms, our proposed zooming algorithm produces the least color artifacts, i.e. the best visual effect.

Finally, the computational complexity analyses of the six concerned algorithms are given and they are measured in terms of the number of operations. These operations include the addition (ADD), the multiplication (MUL), the division (DIV), the comparison (CMP), and taking absolute value (ABS). Although the true number of operations required is dependent on the testing images, for analysis, we assume that the probability of each condition branch in each concerned algorithm is the same. Table IV demonstrates the average number of operations required for demosaicing and zooming a pixel by the three stages in our proposed algorithm. The three stages in Table IV are matched with those in Fig. 2. Table V demonstrates the average number of operations required for demosaicing and zooming a pixel by the six concerned algorithms. Table V indicates that except those of the ADD and ABS operations, our proposed zooming algorithm needs moderate number of the other operations.

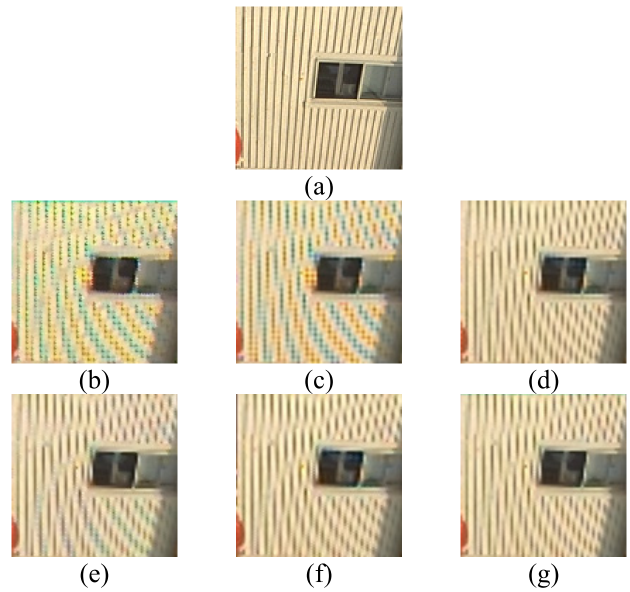

Fig. 15. Seven magnified subimages cut from the testing image No. 19. (a) Original full color image and the zoomed images obtained from (b) A_1, (c) A_2, (d) A_3, (e) A_4, (f) A_5, and (g) our proposed algorithm.

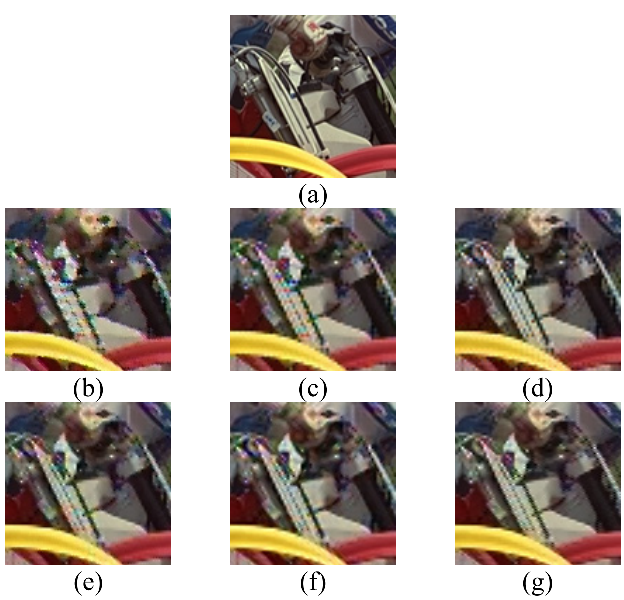

Fig. 14. Seven magnified subimages cut from the testing image No. 5. (a) Original full color image and the zoomed images obtained from (b) A_1, (c) A_2, (d) A_3, (e) A_4, (f) A_5, and (g) our proposed algorithm.

V. CONCLUSION

In this paper, a new joint demosaicing and zooming algorithm for mosaic images has been presented. Based on the extracted more accurate edge information and the color difference concept, the proposed joint demosaicing and zooming algorithm for mosaic images is developed. Further, a new refinement method, which combines the concept of the local color ratios and our proposed proper weighting scheme, is proposed to enhance the quality of the zoomed images. Based on twenty-four popular testing mosaic images, experiments have been carried out to

TABLE V.
AVERAGE NUMBER OF OPERATIONS REQUIRED FOR DEMOSAICING AND ZOOMING A PIXEL IN THE SIX CONCERNED ALGORITHMS.

	ADD	MUL	DIV	CMP	ABS
A_1	102.875	27	26	0	4.5
A_2	122.75	22	45.25	0	16
A_3	88.25	27	16.25	0	0
A_4	81.455	14.625	9.125	5.75	21.5
A_5	77.625	43	6.125	22	0
Ours	135.373	36.958	19.375	13.249	38

Authorized licensed use limited to: National Taiwan Univ of Science and Technology. Downloaded on October 13, 2009 at 22:45 from IEEE Xplore. Restrictions apply.

demonstrate the quality advantage of our proposed joint demosaicing and zooming algorithm in terms of CPSNR, S-CIELAB ΔE^*_{ab} and the color artifacts when compared with several previous zooming algorithms.

REFERENCES

[1] D. Alleysson, S. Susstrunk, and J. Herault, "Linear demosaicing inspired by the human visual system," *IEEE Trans. Image Processing*, vol. 14, no. 4, pp. 439–449, 2005.

[2] B. E. Bayer, "Color Imaging Array," U.S. Patent# 3 971 065, 1976.

[3] H. A. Chang and H. H. Chen, "Stochastic color interpolation for digital cameras," *IEEE Trans. Circuits and Systems for Video Technology,* vol. 17, no. 8, pp. 964–973, 2007.

[4] K. H. Chung and Y. H. Chan, "Color demosaicking using variance of color differences," *IEEE Trans. Image Processing,* vol. 15, no. 10, pp. 2944–2955, 2006.

[5] K. H. Chung and Y. H. Chan, "A low-complexity joint color demosaicking and zooming algorithm for digital camera," *IEEE Trans. Image Processing,* vol. 16, no. 7, pp. 1705–1715, 2007.

[6] K. L. Chung, Y. W. Liu and W. M. Yan, "A hybrid gray image representation using spatial- and DCT-based approach with application to moment computation," *J. of Visual Communication and Image Representation,* vol. 17, no. 6, pp. 1209-1226, 2006.

[7] K. L. Chung, W. J. Yang, W. M. Yan, and C. C Wang, "Demosaicing of color filter array captured images using gradient edge detection masks and adaptive heterogeneity projection," *IEEE Trans. Image Processing,* vol. 17, no. 12, pp. 2356–2367, 2008.

[8] R. Gonzalez and R. Woods, *Digital Image Processing,* Addison Wesley, New York, 1992.

[9] B. Gunturk, Y. Altunbasak, and R. Mersereau, "Color plane interpolation using alternating projections," *IEEE Trans. Image Processing,* vol. 11, no. 9, pp. 997–1013, 2002.

[10] R. W. G. Hunt, *Measuring Colour,* 2nd Ed., Ellis Horwood, Chichester, U. K., 1995.

[11] R. Kimmel, "Demosaicing: image reconstruction from color CCD samples," *IEEE Trans. Image Processing,* vol. 8, no. 9, pp. 1221–1228, 1999.

[12] W. Lee, S. Lee, and J. Kim, "Cost-effective color filter array demosaicing using spatial correlation," *IEEE Trans. Consumer Electronics,* vol. 52, no. 2, pp. 547–554, 2006.

[13] W. Lu and Y. P. Tan, "Color fiter array demosaicking: now method and performance measures," *IEEE Trans. Image Processing,* vol. 12, no. 10, pp. 1194–1210, 2003.

[14] R. Lukac, K. N. Plataniotis, D. Hatzinakos, and M. Aleksic, "A novel cost effective demosaicing approach," *IEEE Trans. Consumer Electronics,* vol. 50, no. 1, pp. 256–261, 2004.

[15] R. Lukac and K. N. Plataniotis, "Normalized color-ratio modeling for CFA interpolation," *IEEE Trans. Consumer Electronics,* vol. 50, no. 2, pp.737–745, 2004.

[16] R. Lukac, K. Martin, and K. N. Plataniotis, "Demosaicked image postprocessing using local color ratios," *IEEE Trans. Circuits and Systems for Video Technology,* vol. 14, no. 6, pp. 914–920, 2004.

[17] R. Lukac, K. N. Plataniotis, and D. Hatzinakos, "Color image zooming on the Bayer pattern," *IEEE Trans. Circuits and Systems for Video Technology,* vol. 15, no. 11, pp. 1475–1492, 2005.

[18] R. Lukac and K. N. Platataniotis, "Digital zooming for color filter array," *Real-Time Imaging,* vol. 11, no. 2, pp. 129–138, 2005.

[19] R. Lukac and K. N. Plataniotis, "Color filter arrays: Design and performance analysis," *IEEE Trans. Consumer Electronics,* Vol. 51, No. 4, pp.1260–1267, 2005.

[20] R. Lukac, K. N. Plataniotis, D. Hatzinakos, and M. Aleksic, "A new CFA interpolation framework," *Signal Processing,* vol. 86, no. 7, pp. 1559–1579, 2006.

[21] K. McLaren, "The development of the CIE 1976 (L*a*b) uniform color-space and colour-difference formula," *Journal of the Society of Dyers and Colourists,* vol. 92, pp. 338–341, 1976.

[22] D. D. Muresan and T. W. Parks, "Demosaicing using optimal recovery," IEEE Trans. Image Processing, vol. 14, no. 2, pp. 267–278, 2005.

[23] S. C. Pei and I. K. Tam, "Effective color interpolation in CCD color filter arrays using signal correlation," *IEEE Trans. Circuits and Systems for Video Technology,* vol. 19, no. 6, pp. 503–513, 2003.

[24] T. Sakamoto, C. Nakanishi, and T. Hase, "Software pixel interpolation for digital still cameras suitable for a 32-bit MCU," *IEEE Trans. Consumer Electronics,* vol. 44, no. 4, pp. 1342–1352, 1998.

[25] C. Y. Su, "Highly effective iterative demosaicing using weighted-edge and color-difference interpolations," *IEEE Trans. Consumer Electronics,* vol. 52, no. 2, pp. 639–645, 2006.

[26] P. Thevenaz, T. Blu, and M. Unser, "Interpolation revisited," *IEEE Trans. Medical Imaging,* vol. 19, no. 7, pp. 739–758, 2000.

[27] X. Wu and N. Zhang, "Primary-consistent soft-decision color demosaicking for digiral cameras (patent pending)," *IEEE Trans. Image Processing,* vol. 13, no. 9, pp. 1263–1274, 2004.

[28] L. Zhang and X. Wu, "Color demosaicking via directional linear minimum mean square-error estimation," *IEEE Trans. Image Processing,* vol. 14, no. 12, pp. 2167–2178, 2005.

[29] L. Zhang and X. Wu, "An edge-guided image interpolation algorithm via directional filtering and data fusion," *IEEE Trans. Image Processing,* vol. 15, no. 8, pp. 2226–2238, 2006.

[30] L. Zhang and D. Zhang, "A joint demosaicking-zooming scheme for single chip digital color cameras," *Computer Vision and Image Understanding,* vol. 107, no. 1–2, pp. 14–25, 2007.

[31] [Online]. Available: http://www.site.uottawa.ca/~edubois/demosaicking/.

[32] [Online]. Available: http://140.118.175.164/WJYang/paper/ZDemo/.

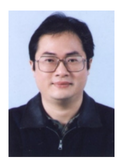

Kuo-Liang Chung (M'91-SM'01) received his B.S., M.S., and Ph.D. degrees in Computer Science and Information Engineering from the National Taiwan University in 1982, 1984, and 1990, respectively. He was a visiting scholar at the University of Washington in the summer of 1999. He was the head of the Department of Computer Science and Information Engineering at the National Taiwan University of Science and Technology from 2003 to 2006. He is now a professor. He was the executive editor of Journal of the Chinese Institute of Engineers from 1996 to 1998. Dr. Chung received the Distinguished Engineering Professor Award from Chinese Institute of Engineers in 2001; received the Distinguished Research Award (2004 to 2007) from the National Science Council, Taiwan, and received the best paper award from the Society of Computer Vision, Graphics, and Image Processing (Taiwan) in 2007. He is a senior member of IEEE and a fellow of IET. He has authored and coauthored over 130 publications in books and international well-known journals. His research interests include image/video compression, image/video processing, pattern recognition, artificial intelligence, algorithms, and multimedia applications.

Wei-Jen Yang received the B.S. degree in Computer Science and Information Engineering from National Taiwan University of Science and Technology, Taipei, Taiwan, in 2004. He is currently pursuing the Ph.D. degree in Computer Science and Information Engineering at National Taiwan University, Taipei, Taiwan. His research interests include color image processing, digital camera image processing, image/video compression, computer vision, pattern recognition, and algorithms.

Pang-Yen Chen received the B.S. degree in Materials Science and Engineering from National Taiwan University, Taipei, Taiwan, in 2006. He received the M.S. degree in Computer Science and Information Engineering from National Taiwan University, Taipei, Taiwan, in 2008. His research interests include digital camera image processing, computer vision, numerical linear algebra, pattern recognition, and algorithms.

Authorized licensed use limited to: National Taiwan Univ of Science and Technology. Downloaded on October 13, 2009 at 22:45 from IEEE Xplore. Restrictions apply.

Wen-Ming Yan received the B.S. and M.S. degrees in Mathematics from National Taiwan University, Taipei, Taiwan. Now, he is an Associate Professor in Computer Science and Information Engineering at National Taiwan University. His research interests include scientific computation, image compression, computer vision, numerical linear algebra, image processing, coding theory, and algorithms.

Chiou-Shann Fuh (S'89-M'95) received the B.S. degree in computer science and information engineering from National Taiwan University, Taipei, Taiwan, R.O.C., in 1983, the M.S. degree in computer science from The Pennsylvania State University, University Park, in 1987, and the Ph.D. degree in computer science from Harvard University, Cambridge, MA, in 1992. He was with AT&T Bell Laboratories, Murray Hill, NJ, where he was engaged in performance monitoring of switching networks from 1992 to 1993. He was an Associate Professor in the Department of Computer Science and Information Engineering, National Taiwan University, Taipei, Taiwan, from 1993 to 2000, and then was promoted to Full Professor. His current research interests include digital image processing, computer vision, pattern recognition, and mathematical morphology.

Authorized licensed use limited to: National Taiwan Univ of Science and Technology. Downloaded on October 13, 2009 at 22:45 from IEEE Xplore. Restrictions apply.